Proceedings of the ASME 2010 3rd Joint US-European Fluids Engineering Summer Meeting and 8th International Conference on Nanochannels, Microchannels, and Minichannels
FEDSM-ICNMM2010
August 1-5, 2010, Montreal, Canada

FEDSM-ICNMM2010-31037

COMPUTATIONAL INVESTIGATION OF LIQUID SPRAY DISPERSION MODIFICATION BY CONICAL NOZZLE ATTACHMENTS

Konstantin Pougatch
University of British Columbia
Department of Mechanical Engineering
2054-6250 Applied Science Lane
Vancouver, BC, Canada
pougatch@mech.ubc.ca

Martha Salcudean
University of British Columbia
Department of Mechanical Engineering
2054-6250 Applied Science Lane
Vancouver, BC, Canada
msal@interchange.ubc.ca

ABSTRACT

Liquid sprays characteristics such as the droplet size and the dispersion angle are determined by the atomizer design and the physical properties of the liquid and the surrounding gas. One of the options to change these characteristics is to attach a specially designed piece to the nozzle exit. While there can be a variety of shapes of such attachments, we chose a conical geometry to exploit its axial symmetry and, at the same time, obtain the results that can be generalized to other configurations. Thus, we investigate an addition of the conically shaped attachment to the premixed gas-assisted high-pressure atomizer with the previously developed numerical model. It is a two-fluid Eulerian-Eulerian model with a catastrophic phase inversion that was developed for compressible gas-liquid mixtures and can be applied to both the flow through the nozzle-atomizer and to the dispersion of the spray. The model also accounts for the break-up and coalescence effects of bubbles and droplets.

Our investigation reveals that the conical nozzle attachments act as spray limiters by reducing the natural expansion angle of a spray. Also, the droplets produced by the nozzle with a conical addition tend to be larger than the ones obtained with a stand alone nozzle. The largest droplets were generated by the smallest attachment angle considered – 10º. With the increase of the angle, the spraying characteristics become closer to the ones of the stand alone nozzle. It can be concluded that the conical shape of the attachments with a relatively small angle may be used when higher jet penetration and lower dispersion are desirable. The attachments with larger angles do not offer a substantial difference from the stand alone nozzle. Another important conclusion is that the dispersion of the jet is determined by the radial momentum transferred to the liquid before or immediately after the phase inversion takes place. Thus, for improved dispersion, the area where the atomization is taken place should not be restricted.

INTRODUCTION

Many industrial processes utilize liquid sprays due to their high surface area to volume ratio. Whether it is to quickly deliver a reagent into the reaction zone, to start a granulation process, to combust liquid fuel, or to provide rapid cooling, sprays are essential to the process performance. The sprays are usually obtained by atomizing, or breaking-up, liquid in a special device called a nozzle. With such a large variety of nozzle applications, it is not surprising that there is also a large variety of nozzle designs. They range from a simple orifice, through which the liquid is pushed, to more sophisticated systems involving pressurized liquid delivered into the swirling gas.

One of the designs involves the gas injection into the pressurized liquid flowing in a pipe and subsequent passing of the mixture through the convergent-divergent nozzle [1]. The atomization takes place close to the nozzle exit due to the rapid expansion of the gaseous phase following a significant pressure drop. This type of nozzle found its application in bitumen injection into the fluid coking reactor – a fluidized

bed of hot coke particles designed to break the bitumen down to lighter hydrocarbons to be subsequently used as a substitute for conventional oil [2].

It is beneficial from the process development point of view to have some control over jet penetration and jet dispersion. Basically, the jet penetration describes how long the jet is and the jet dispersion – how wide it is. As the momentum of the jet is conserved, the penetration and dispersion are generally inversely varying parameters. One of the means to control the jet dispersion without changing the nozzle itself is an installation of an axially aligned spray modifier attachment to the exit of the nozzle. The dispersion and penetration as well as other spray properties such as the droplet sizes and the liquid flux distribution, are affected by the addition of such a modifier. Even though there can be a variety of modifier shapes including the ones with azimuthal profile variations, we concentrate on the simple conical design that allows for an investigation of the changes that the attachment brings to the flow and has an inherent axial symmetry. While our intuition based on the fan nozzles performance suggests that the spray simply follows the angle of the nozzle, this is not the case in the described nozzles because of a number of reasons discovered during the analysis. We utilize the recently developed mathematical model [3] to provide a closer look at the flow features and to investigate the influence of differently angled conical attachments on the sprays they produce and gain insights into their performance.

MODEL DESCRIPTION

An Eulerian-Eulerian multi-fluid model previously developed by Pougatch et al. [1, 3] for gas-assisted atomization and spray dispersion is used for numerical simulations. The model is applicable for both liquid-continuous bubble-dispersed and gas-continuous droplet-dispersed flow regimes that can exist simultaneously in the different parts of the computational domain. Particle size distribution is accounted for by a monodispersed particle distribution assumption. That is, the variety of sizes of particles, which are assumed to be spherical, is represented by a local average particle diameter that varies throughout the flow field. Such approach is similar to the population balance model with only one bin of particles. The model does not include mass or heat transfer. The model was validated based on the pressure measurements along the nozzle wall [1], water fluxes measurements across the spray at different distances from the nozzle orifice [3], and as a part of a larger model, based on the experiments of ethanol dispersion in a fluidized bed [4].

CONSERVATION EQUATIONS

The model is based on the ensemble averaged (see [5]) mass and momentum conservation equations written for the continuous (c) and dispersed (d) phases.

$$\frac{\partial}{\partial t}\alpha_i\rho_i + \nabla\cdot\alpha_i\rho_i\mathbf{V}_i = 0 \qquad i = c,d \tag{1}$$

$$\frac{\partial}{\partial t}\alpha_i\rho_i\mathbf{V}_i + \nabla\cdot\alpha_i\rho_i\mathbf{V}_i\mathbf{V}_i = \nabla\cdot\boldsymbol{\tau}_i - \alpha_i\nabla P_i + \sum_k \mathbf{F}_i^k \qquad i = c,d \tag{2}$$

As it was previously shown that the gravity influence is relatively small inside the nozzle [1] and negligible for more than one meter distance from the nozzle orifice in the spray [3], the gravity term in the momentum equations is omitted. The non-viscous part of the stress tensor is calculated based on the Boussinesq approximation extended to multi-phase flows.

$$\boldsymbol{\tau}_i^t = \alpha_i\mu_i^t\left(\left(\nabla\mathbf{V}_i + \nabla\mathbf{V}_i^{\mathrm{T}}\right) - \frac{2}{3}\mathbf{I}\nabla\mathbf{V}_i\right) - \frac{2}{3}\alpha_i\rho_i k_i\mathbf{I} \qquad i = c,d \tag{3}$$

While the energy conservation equation is necessary to account for compressibility effects in the gaseous phase near the nozzle orifice where the gas velocity is relatively high, viscous heat dissipation can be ignored, and in the absence of heat transfer through the boundaries, the energy equation simplifies to the requirement for the total gas enthalpy to be constant.

$$\frac{dH_g}{dt} = \frac{d}{dt}\left(c_{p_g}T_g + \frac{\mathbf{V}_g^{\,2}}{2} + k_g\right) = 0 \tag{4}$$

The variation of the average particle diameter introduced above is determined by the particle number density conservation. The transport equation for the particle number density defined as

$$n = \frac{6\alpha_d}{\pi d^3} \tag{5}$$

takes the following form [6]

$$\frac{\partial n}{\partial t} + \nabla\cdot\left(\mathbf{V}_d n\right) = \nabla\cdot\left(\frac{\mu_d^t}{\rho_d Sc^t}\nabla n\right) + n\left(f_{br} - f_{coal}\right) \tag{6}$$

The source terms on the right hand side resulting from the breakage and coalescence of particles need to be separately defined. The atomization is modeled as a catastrophic phase inversion that depends only on the local values of the volume

fraction. That is, the locally continuous phase is determined based on the critical value of the volume fraction. This critical value, 80%, was previously obtained during the process of model validation for air-assisted water atomization [3].

CONSTITUTIVE EQUATIONS

The main equations written above require additional sub models to determine stress tensor and interfacial forces. As the detailed descriptions of all sub-models are available in [3], in this paper we provide only a shortened version to introduce all of them.

Interfacial forces

Among the variety of possible interfacial forces, we consider drag, turbulent dispersion, and virtual mass. The drag is calculated as

$$\mathbf{F}_d^{drag} = \frac{3}{4}\frac{\alpha_d \rho_c C_D}{d}\left|\mathbf{V}_c - \mathbf{V}_d\right|\left(\mathbf{V}_c - \mathbf{V}_d\right); \quad \mathbf{F}_c^{drag} = -\mathbf{F}_d^{drag} \tag{7}$$

Depending on the flow regime, i.e. nature of the continuous phase and its volume fraction, different correlations are used for the drag coefficient. Violet and Simonin [7] model is utilized for the turbulent dispersion.

$$\mathbf{F}_d^{disp} = \frac{3}{4}\frac{\alpha_c \alpha_d \rho_c C_D}{d}\left|\mathbf{V}_c - \mathbf{V}_d\right|\mathbf{V}_{drift} \qquad \mathbf{F}_c^{disp} = -\mathbf{F}_d^{disp} \tag{8}$$

Where the drift velocity is defined as

$$\mathbf{V}_{drift} = \frac{\mu_m^t}{\rho_m Sc^t}\left(\frac{\nabla\left(\rho_c \alpha_c\right)}{\rho_c \alpha_c} - \frac{\nabla\left(\rho_d \alpha_d\right)}{\rho_d \alpha_d}\right) \tag{9}$$

The virtual mass force arises due to acceleration of the continuous phase in the wake of the particle. This force is important whenever the density of the continuous phase is significantly larger than the one of the dispersed phase.

$$\mathbf{F}_d^{vm} = C_{vm}\alpha_d \rho_c\left[\left(\frac{\partial \mathbf{V}_c}{\partial t} + \mathbf{V}_c \cdot \nabla \mathbf{V}_c\right) - \left(\frac{\partial \mathbf{V}_d}{\partial t} + \mathbf{V}_d \cdot \nabla \mathbf{V}_d\right)\right] \tag{10}$$
$$\mathbf{F}_c^{vm} = -\mathbf{F}_d^{vm}$$

The value of the virtual mass coefficient varies with the volume fraction.

Turbulence modeling

To describe a fluctuating motion of the particular phase we adopted the mixture turbulent model developed by Behzadi et al. [8]. It is basically an extension of k-epsilon model to the multiphase flow with an assumption that fluctuation velocities of both phases are directly proportional with a proportionality constant being called a response coefficient.

$$\mathbf{v}_d' = C_t \mathbf{v}_c' \tag{11}$$

Such an assumption allows for summation of all phase turbulence equations to obtain a single set of equations for the mixture turbulent kinetic energy and its dissipation rate.

$$\frac{\partial}{\partial t}\left(\rho_m k\right) + \nabla \cdot \left(\rho_m \mathbf{V}_m k\right) = \nabla \cdot \frac{\mu_m}{\sigma_k}\nabla k + Q - \rho_m \varepsilon + S \tag{12}$$

$$\begin{aligned} &\frac{\partial}{\partial t}\left(\rho_m \varepsilon\right) + \nabla \cdot \left(\rho_m \mathbf{V}_m \varepsilon\right) = \\ &= \nabla \cdot \frac{\mu_m}{\sigma_\varepsilon}\nabla \varepsilon + \frac{\varepsilon}{k}\left(C_{\varepsilon 1} Q - C_{\varepsilon 2}\rho_m \varepsilon + C_{\varepsilon 3} S\right) \end{aligned} \tag{13}$$

For calculation of the response coefficient defined in Eq. (11), we used the model developed by Viollet and Simonin [7].

Break-up and coalescence

We account for the break-up of particles due to two mechanisms: the interfacial and turbulent shear. The particle breaks-up if the shear forces exceed surface tension forces that keep the particle together. For bubbles break up we modified the Martinez-Bazan et al. [9] model of break-up frequency

$$f_{br} = K\frac{\sqrt{\left(V^{rel}\right)^2 - \frac{12\sigma}{\rho_c d}}}{d} \tag{14}$$

by using the largest from the slip and fluctuation velocities, i.e.

$$\left(V^{rel}\right)^2 = \max\left\{\beta\left(\varepsilon d\right)^{2/3}; \left(\mathbf{V}_c - \mathbf{V}_d\right)^2\right\} \tag{15}$$

For droplets break up we extended the Kolev's model [10] to include the turbulent induced break-up by introducing an additional maximum stable droplet diameter, which is obtained from the critical turbulent Weber number $\left(We = \rho_c\left(V^{rel}\right)^2 d/\sigma\right)$. The latter is determined from the relation suggested by Kocamustafaogullari et al. [11] connecting drag and turbulent critical Weber numbers.

$$We_{cr}^{turb} = \left(\frac{\rho_c}{\rho_d}\right)^{\frac{2}{3}}\frac{\left(\rho_d - \rho_c\right)}{\rho_d}We_{cr}^{drag} \tag{16}$$

The coalescence may take place following particle collisions. Thus, the coalescence frequency is determined from the collision frequency and the coalescence probability.

Boundary conditions

At interfacial boundaries between gas and liquid, the normal stresses are balanced with the surface tension forces. At all walls, the multiphase wall functions proposed in [1] are applied to calculate the wall shear stress and the turbulence quantities. Fixed flow rates of liquid and gas are assumed at the inlet; therefore, the inlet pressure and volume fractions are calculated as a part of the solution.

NUMERICAL METHOD

The conservation equations are discretized by a control volume method with second order spatial discretization schemes and solved transiently. In order to account for a strong interfacial coupling due to the virtual mass and interfacial drag forces, the pressure based IPSA coupling procedure for multiphase flow developed by Spalding [12] is implemented. That is, the momentum equations for all phases are assembled in a single matrix and solved simultaneously by GMRES method. Next, the total volume conservation equation (the sum of Eq. (1) for gas and liquid phases) is used to obtain the velocity and pressure corrections. The numerical procedure is detailed in [1].

RESULTS AND DISCUSSION

DESCRIPTION OF CASES

We consider a standard TEB-type nozzle with a conical attachment as shown in Fig. 1. This nozzle itself was previously investigated in [3].

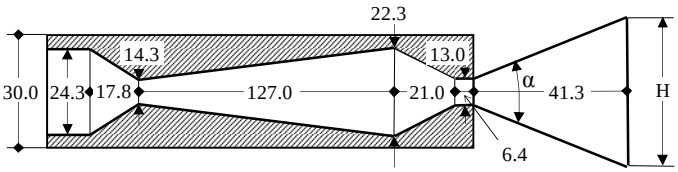

Figure 1 Nozzle with an attachment schematics (mm, not to scale).

While the length of the attachment is fixed, several values of its expansion angle are studied. They are listed in Table 1 together with a corresponding height of the attachment exit. In addition, we also include a case without an attachment, that can also be viewed as having an attachment with an expansion angle of 180º, for comparative purposes.

Air and water are used as working fluids. The air flow rate is 0.0442 kg/s and the water flow rate is 2.2 kg/s; it corresponds to GLR (Gas to Liquid mass Ratio) of 2%. The room temperature, 20ºC, and the atmospheric pressure, $1.01325 \cdot 10^5$ Pa, are set as the ambient conditions. All physical properties of materials, such as water surface tension (0.0727 N/m) and water density (1000 kg/m^3), are taken at these conditions.

Table 1 Attachment expansion angle and exit height of the investigated cases.

Case #	α, degrees	H, mm
1	180	0
2	10	20.2
3	20	27.6
4	40	43.1
5	60	60.7
6	80	82.3

COMPUTATIONAL GRID

The computational domain is axisymmetric and includes the nozzle and its surrounding areas where the spray is dispersed. The domain extends axially 1 m from the nozzle exit and radially – 0.2 m from the axis. In addition, a short piece of pipe (0.2 m) with the same diameter as the nozzle inlet is added in front of it to allow for some flow development before the mixture enters the nozzle.

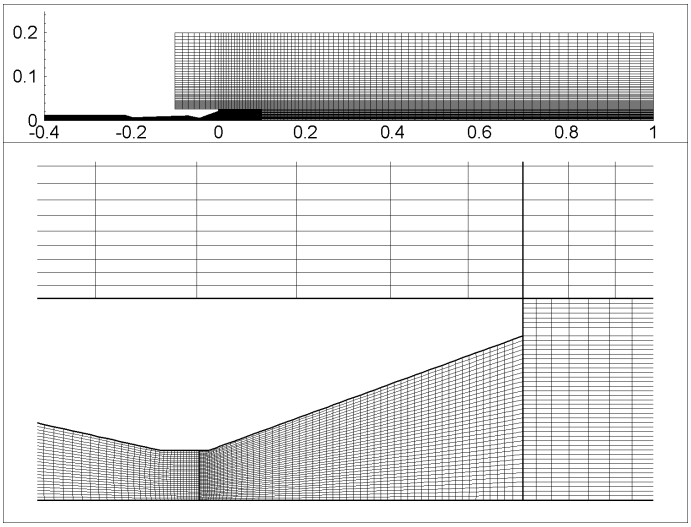

Figure 2 Computational grid and domain segmentation (full domain – above, and nozzle attachment area – below).

A multi-segment curvilinear non-uniform grid, shown in Fig. 2, is developed to provide a good resolution in the areas of high flow gradients – nozzle, attachment and its immediate vicinity – and, at the same time, to allow for practical computations. The grid contains about 11 000 grid cells, more for the larger expansion angles, less for the smaller ones. The

modeling set up and the grid density are very similar to the ones previously used [3]. As it was already established that such resolution provides a grid independent solution, no additional grid independence studies are conducted.

FLOW ANALYSIS

All the considered cases are simulated, and the transient converged solutions are obtained with a time step of 0.02 ms. While the solutions are time-dependant, the variations of the flow parameters in time are generally very small rendering a steady flow for practical purposes. These minor variations have a time-scale about 1 ms. It is interesting to note that the time-dependencies in the cases with the nozzle attachment are even less than the fairly small ones observed for the stand alone nozzle case; therefore, it follows that an attachment has some stabilizing effects. The subsequent analysis is done for the results averaged during 20 ms of real time.

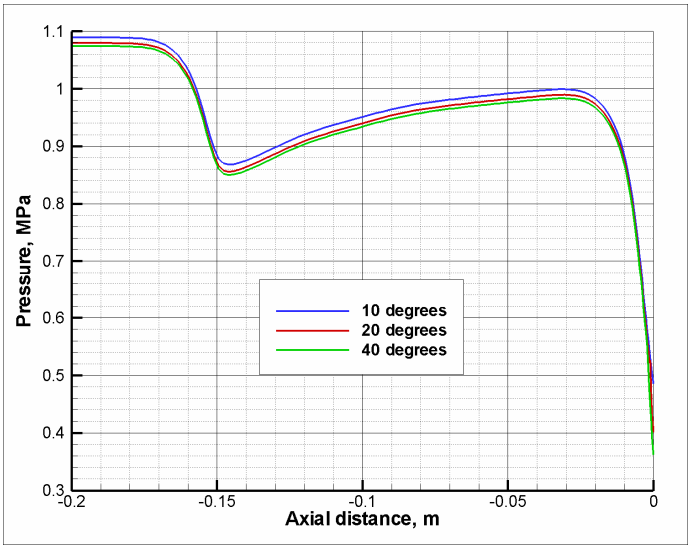

Figure 3 Pressure variation along the nozzle centerline for various cases.

We start the analysis with comparing flows inside the nozzle. Figure 3 presents the pressure profiles along the centerline of the nozzle for several cases with a varying expansion angle. While an overall shape of the profile is very similar for all cases, quite naturally, the smaller expansion angles result in the larger pressure drops through the nozzle because of the added resistance to the flow. The difference, however, is too small (less than 1%) to have any practical consequences. Moreover, this difference rapidly decreases as the expansion angle increases: the curves for the 60 and 80 degree cases as well as for a stand alone nozzle virtually coincide with the 40 degree case curve and are not shown in the graph. All other flow properties, such as the velocities, the bubble average diameter and the volume fraction, show even less dependency on the expansion angle or the existence of the spray modifier. Therefore, in the following we focus our attention on the flow outside of the nozzle and in the spray modifier itself.

The droplet volume fraction distribution in the nozzle and in the spray is shown in Fig. 4 for all cases. Note that in order to improve presentation, these and subsequent plots are extended to the full axial cross-section based on axial symmetry. As it was already observed in the previous paragraph, inside the nozzle the volume fraction distribution does not appreciably change with the addition of the modifier. While a minor difference in the pressure does influence volume fractions, this influence is very small. At the same time, immediately after the nozzle exit, the presence of the narrow modifier visibly alters the flow. We can see that for the cases with 10º and 20º angle larger volume fractions of water are present after the nozzle exit due to the delay of the air expansion by the modifier geometry. This in turn results in the delayed atomization for the narrow angle cases. Figure 5 shows phase inversion surfaces for all cases. Evidently, the location for the atomization moves downstream with narrowing of the expansion angle. However, for angles 40º and above no influence is observed. The spray structure is generally similar to the one previously observed for these types of nozzles [3]. Fairly rapid initial rate of the spray dispersion decreases as the droplets move further away from the nozzle. It is evident that the addition of the narrow angle attachments significantly modifies the spray. The cases with 10º and 20º angle demonstrate visibly less dispersion than others, the stand alone nozzle case included. We can see that for the narrow attachments, the maximum jet dispersion angle approximately coincides with the angle of the nozzle attachment. Thus, narrowing the angle of the attachment cone produces the less dispersed and, hence, more penetrating jets. The reverse, however, is not true. As soon as the expansion angle reaches about 40º, the spray stops changing and the droplets spatial distribution looks very similar for the cases 40º, 60º, 80º, and for the stand alone nozzle case. It looks as there is a natural expansion angle, which is achieved in a stand alone nozzle that cannot be exceeded. Another interesting observation pertains to the rate of the jet expansion. We can see that for the stand alone nozzle and for the nozzles with wide attachments the expansion rate is relatively large at the beginning and then decreases as the liquid moves further from the nozzle. For the nozzles with narrow attachments, on the other hand, the jet expansion rate remains almost steady throughout the computational domain for 10º case and barely noticeable for 20º case. This phenomenon will be explained later after we examine droplet size variations.

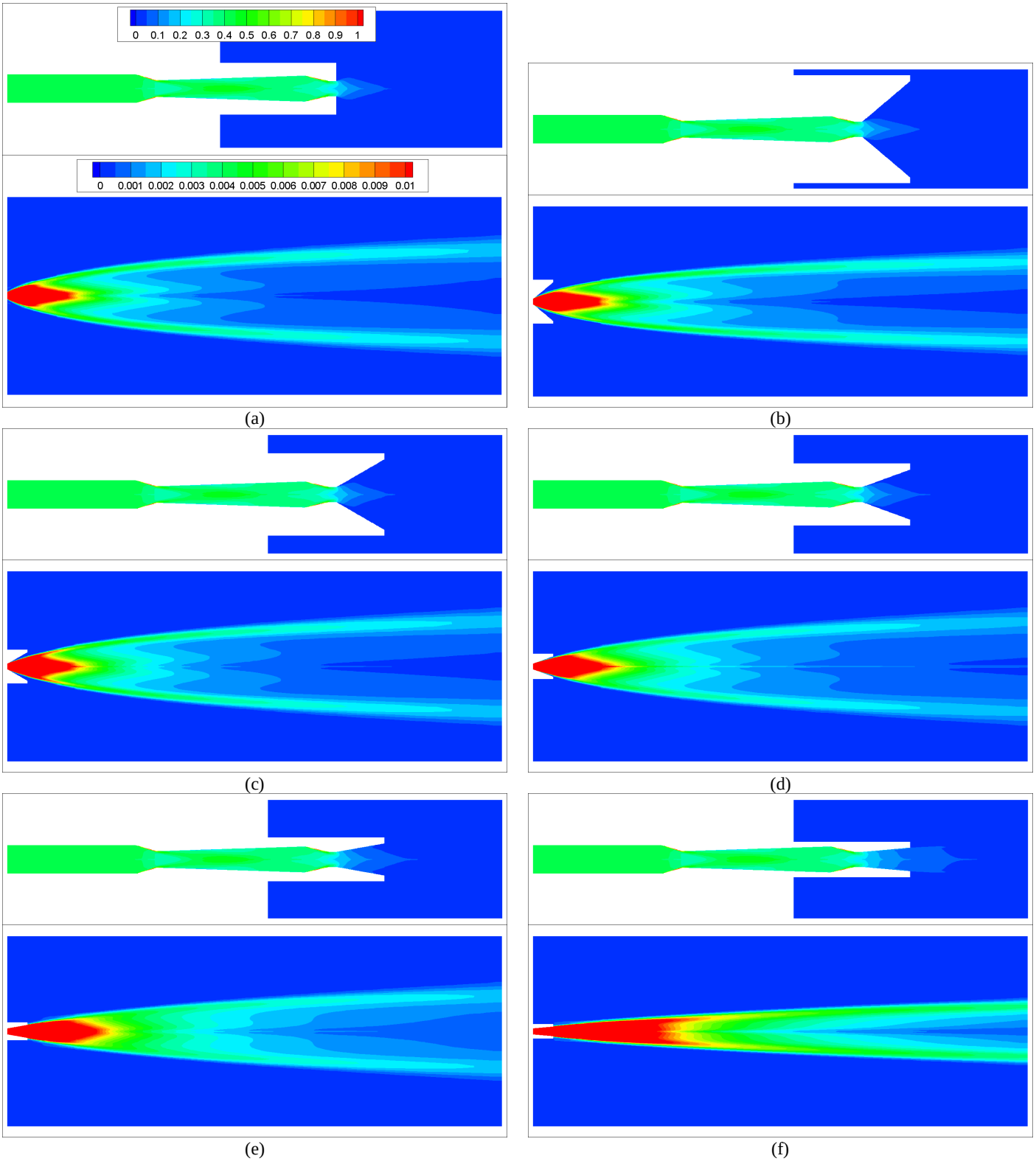

Figure 4 Droplets volume fraction contours in the nozzle and spray modifier (above) and in the spray area (below) for (a) -stand alone nozzle, (b) - 80º, (c) - 60º, (d) - 40º, (e) - 20º, (f) - 10º. Note the different scale for the above and below plots.

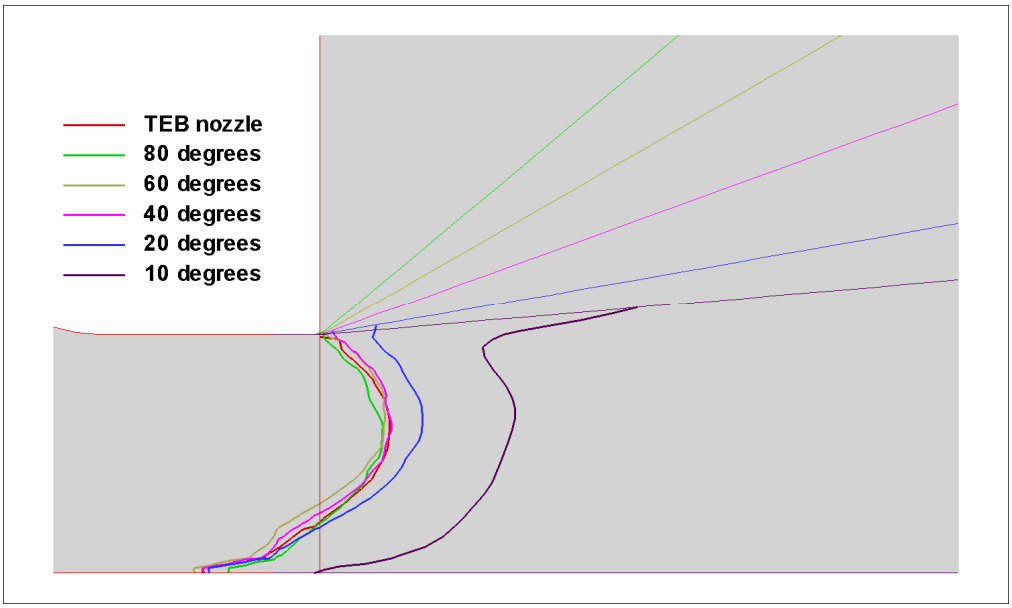

Figure 5 Phase inversion surfaces for all investigated cases.

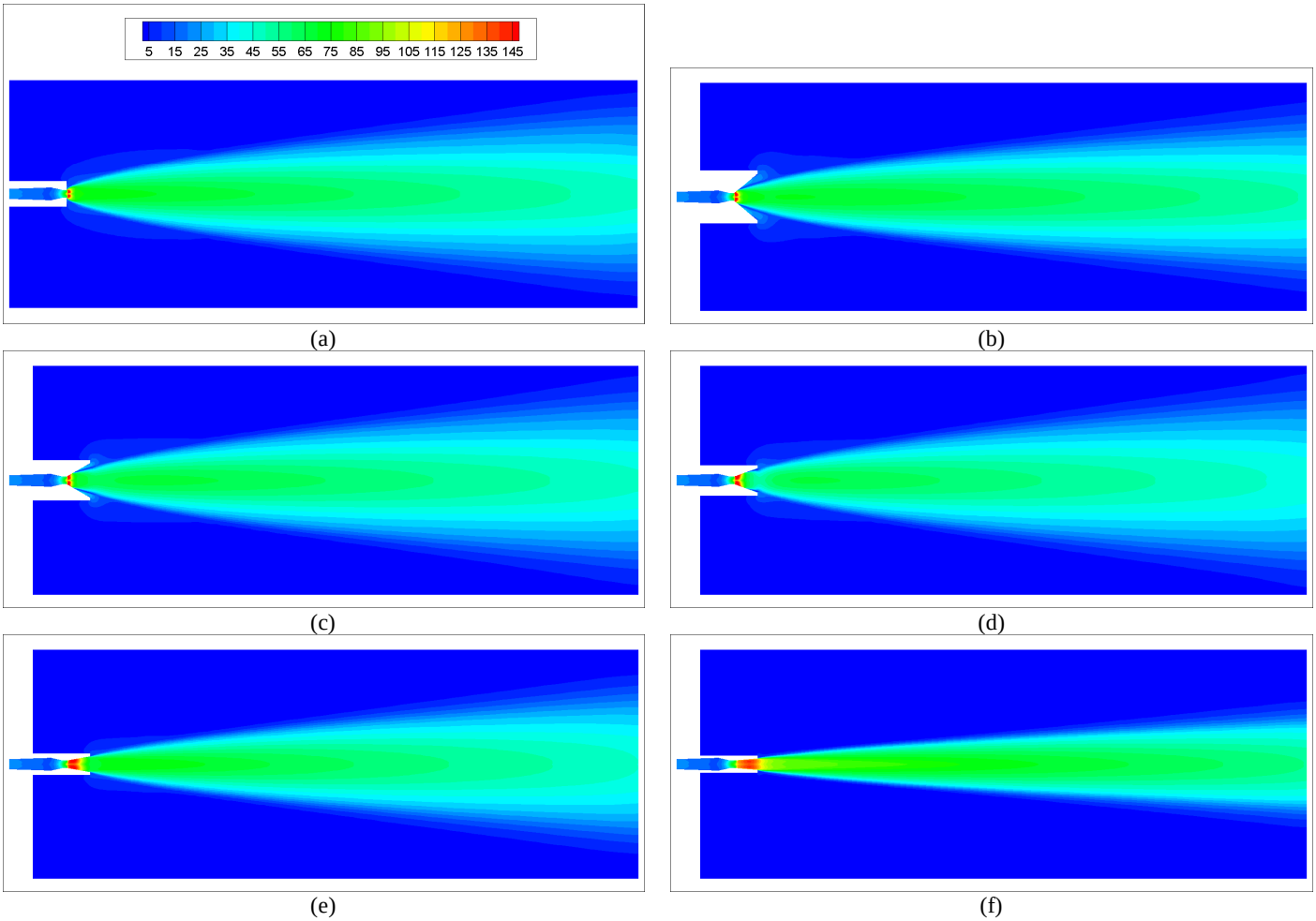

(a) (b)

(c) (d)

(e) (f)

Figure 6 Air velocity magnitude contours in the spray area for (a) -stand alone nozzle, (b) - 80º, (c) - 60º, (d) - 40º, (e) - 20º, (f) - 10º (in m/s).

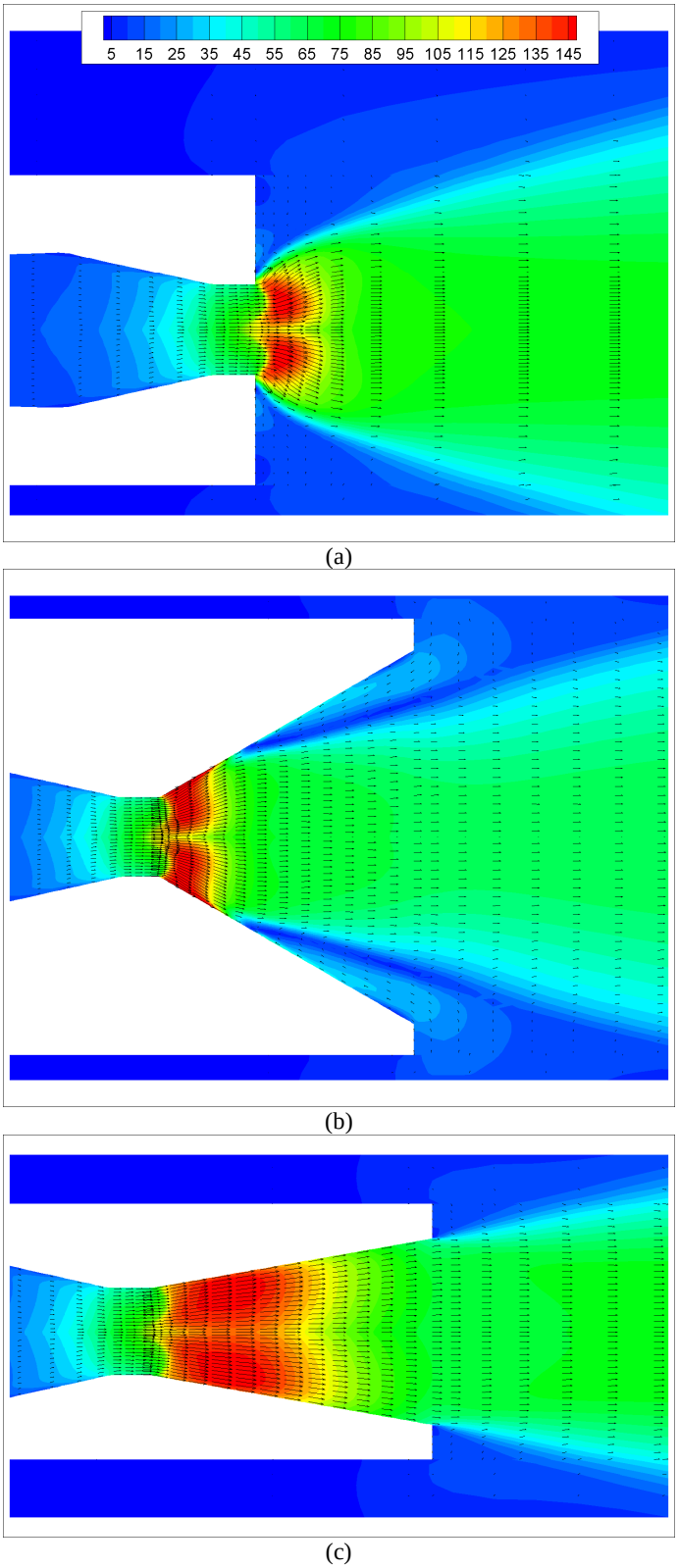

Figure 7 Air velocity vectors and magnitude contours in the nozzle exit area for (a) -stand alone nozzle, (b) - 60º, (c) - 20º (in m/s).

Figure 6 shows the air velocity magnitude for all cases. Evidently, the velocity is the largest for the smallest expansion angle case reconfirming our conclusion about the larger jet penetration for the narrower attachments. These plots also show a high velocity area (red-colored) that immediately follows the atomization. The origin of this area lays in the dramatic difference of the interfacial drag and virtual mass forces between liquid and bubbles and between gas and droplets. Therefore, the atomization results in a significant reduction of the interfacial forces; thus, gas can accelerate allowing the slip velocity, which is the difference between the gas and liquid velocities, to grow. However, this growth is not limitless and at some distance downstream the new equilibrium conditions are reached. This zone, as well as the whole liquid-continuous area preceding it, is characterized by the high interfacial momentum exchange. It is there that the spray droplets obtain the momentum to continue along their trajectories.

We look closer into this area by plotting the velocity vectors in this region in three representative cases (Fig. 7). It can be seen that while in the stand alone nozzle case there is a rapid increase of the radial velocity, in the case with 10º expansion angle the radial velocity changes are rather small. The reason is that without an attachment the jet expands freely in the open air; with the nozzle attachment, however, the expansion takes place inside the spray modifier and it is restricted by its walls. Thus, in the narrow attachment cases the radial velocity is limited by the expansion angle. In the case of the wide attachment angle, shown in Fig.7 (b), the air radial velocity initially grows so that the jet fills the entire area. However soon after, the radial velocity reduces and the jet detaches from the wall. That probably occurs because of the presence of the droplets with relatively large inertia that makes them unable to follow sharp bends in the gas streamlines; the droplets transfer their momentum to the gas through the interfacial forces. As a result, we can observe a recirculation bubble forming near the wall of the expanding section. Note that the recirculation takes place only for the air – the droplets do not really occupy this area (see Fig. 4 (c)) and the existing few continue their movement in the flow direction.

Next, we look at the radial distributions of the liquid flow rates, which are defined as $\varepsilon_l \rho_l \mathbf{V}_l \cdot \mathbf{k}$, for all cases. Figure 8 presents water flow rate variations at 0.3048 m distance from the nozzle exit orifice. As expected, we observe higher flow rates and less dispersion for jets obtained with a narrow nozzle attachment. For the case with 10º angle, the maximum flow rate increases more than three times compared with the stand alone nozzle. What is interesting in this graph is that while almost all cases seem to follow the pattern just described – the reduction of the jet dispersion and the

increase of the maximum flow rate – the case with 80º angle produces a narrower jet than the one obtained with 60º modifier. In order to explain such behavior, we examine the droplet diameter variations in the spray.

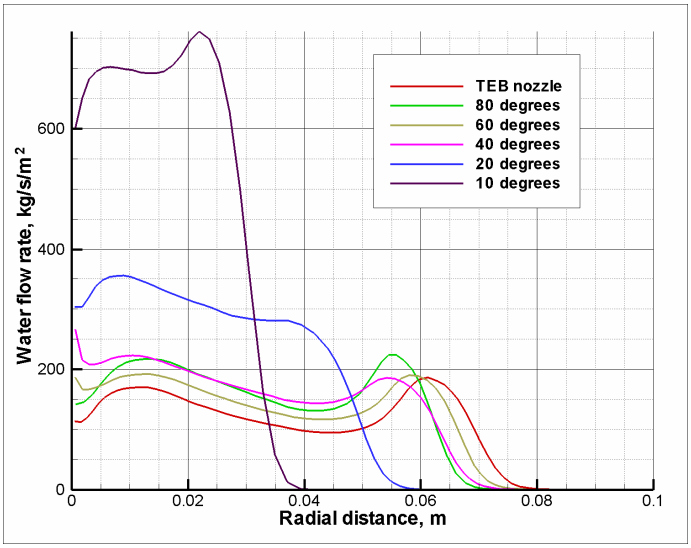

Figure 8 Water flow rates profiles in a radial cross-sectional plane located at 0.3048 m from the nozzle exit

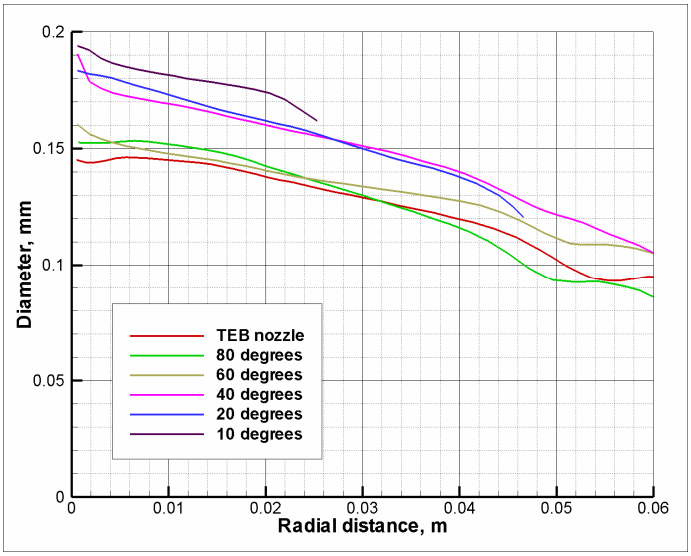

Figure 9 Average droplet diameter variation in a radial cross-sectional plane located at 0.3048 m from the nozzle exit

Figure 9 shows the local average droplet diameter profiles at a 0.3048 m distance from the nozzle exit. First of all, we can see that for all of the cases the average droplet diameter decreases from the axis towards the periphery of the jet. The addition of the spray modifier does not change this trend. Second, the nozzles with the narrow attachments (10º – 40º angle) produce larger droplets than the nozzles with the wide attachments or without any attachments at all. This explains the difference in the spray expansion rate noticed during the analysis of water volume fractions. The reduction of the spray expansion rate as it moves further out from the nozzle is caused by the interfacial friction between the droplets and the air entrained into the jet to preserve the total volume continuity. Therefore, the radial momentum of the droplets is reduced. However, the interfacial friction depends on the droplet size – the larger the droplet, the smaller the friction force. Thus, the sprays with the larger droplets exhibit less momentum exchange, and, hence, less reduction of the expansion rate. Third, we can see that for the 80º angle case, the average droplet diameters at the periphery of the jet are smaller than for all others cases including the stand alone nozzle case. As it was just analyzed, these smaller diameters result in a larger reduction of the jet expansion rate and, ultimately, in a narrower spray. That is in agreement with our earlier observation regarding a perceived anomaly of a somewhat narrower spray for 80º angle case.

To understand the mechanisms underlying the droplet diameter distribution, we need to recall that (a) the droplets are born after the phase inversion and (b) they undergo break-up and coalescence. As the flow in the nozzle is essentially the same for all cases, the average bubble diameter leading to the phase inversion is also essentially the same. Therefore, the initial droplet diameters are also almost the same for all cases. Thus, the differences between the cases appear because of the different break-up rates for the cases with the different nozzle attachments. In our model, the break-up takes place due to either the interfacial shear or the turbulence fluctuations. Previous analysis in [3] confirmed that the dominant breakage mechanism in this type of sprays is the turbulence induced break-up. Therefore, to understand the differences in the break-up rates, we plot contours of the turbulent kinetic energy in Fig. 10. In all of the cases, we can see a substantial turbulence generated near the nozzle exit that propagates downstream dissipating along the way. One can observe that the turbulence is much less for the narrow attachment cases. Probably, this is a consequence of the phase inversion taking place in the restricted environment where the shearing motion induced by the jet is constrained. With smaller turbulence, the break-up frequency is also smaller, and as a result, the droplets are larger.

In addition, we can see a significant amount of turbulence generated in the expansion section of 80º angle case. This turbulence is generated because of the significant air recirculation that takes place near the modifier walls (see Fig. 7 (b)); such recirculation is absent in the stand alone nozzle case. Even though in the stand alone nozzle much turbulence is generated around the sharp angles surrounding the nozzle orifice, at the periphery of the jet it is still less than what is generated by the strong recirculation in the 80º angle case. This is the cause of the smaller droplets being present at

the outer side of the jet and of the unexpected trend of the liquid flow rates for the 80º angle case.

CONCLUSION

The influence of the addition of the spray modifiers to the standard TEB-type nozzle was investigated numerically for water spraying assisted by air. Conical modifiers were chosen for our study. It was discovered that the spray modifiers act as spray limiters by reducing the spray's natural expansion angle. Also, the droplets produced by the nozzle with an addition tend to be larger than the ones obtained with a stand alone nozzle. The largest droplets (~ 190 µm) were generated by the smallest modifier angle considered - 10º. With the increase of the modifier angle the spraying characteristics become closer to the ones of the stand alone nozzle. It can be concluded that the conical shape of the modifiers with a relatively small angle may be used when a higher jet penetration and a lower dispersion is desirable. The modifiers with the larger angles do not offer a substantial difference from the non-modified nozzle. Another important conclusion is that the dispersion of the jet is determined by the radial momentum provided to the liquid before and immediately after the phase inversion takes place. Thus, for improved dispersion, the place where the phase inversion occurs should not be restricted.

An additional interesting observation is that the case with 80º expansion angle differs slightly from the others in terms of the jet expansion and droplet sizes due to the large turbulence generated in the air recirculation area confined within a modifier cone.

ACKNOWLEDGMENTS

The financing for this work was provided by Natural Sciences and Engineering Research Council of Canada (NSERC) and Syncrude Canada Ltd. Authors are grateful to Ed Chan at Syncrude Canada Ltd. and Darwin Kiel and Jonathan Tyler at Coanda Research and Development Corporation for many helpful discussions.

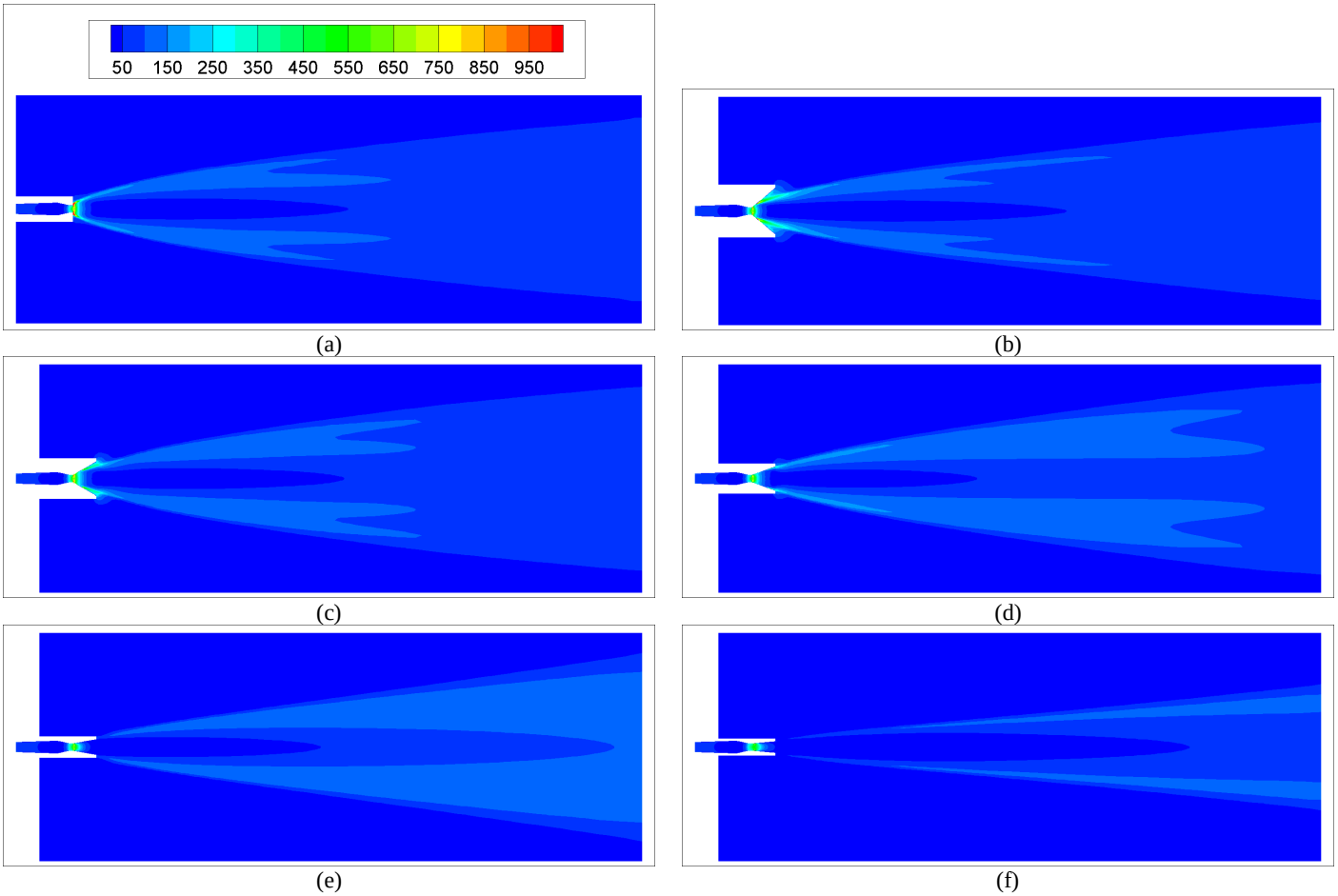

Figure 10 Turbulence kinetic energy contours in the spray area for (a) -stand alone nozzle, (b) - 80º, (c) - 60º, (d) - 40º, (e) - 20º, (f) - 10º (in m^2/s^2).

NOMENCLATURE

c_p	Specific heat, J/kg K
C_D	Drag coefficient, dimensionless
C_t	Response coefficient, dimensionless
C_{vm}	Virtual mass coefficient, dimensionless
$C_{\varepsilon 1}$	Constant in Eq. (13), dimensionless, $C_{\varepsilon 1} = 1.44$
$C_{\varepsilon 2}$	Constant in Eq. (13), dimensionless, $C_{\varepsilon 2} = 1.92$
$C_{\varepsilon 3}$	Constant in Eq. (13), dimensionless, $C_{\varepsilon 3} = 1.2$
d	Locally averaged particle diameter, m
f	Frequency, 1/s
$\mathbf{F}$	Force, N
H_g	Total gas energy, J/kg
$\mathbf{I}$	Unit tensor, dimensionless
k	Turbulent kinetic energy, m^2/s^2
$\mathbf{k}$	Unit vector collinear with axis and oriented in the flow direction
K	Constant in Eq. (14), dimensionless, $K = 0.25$
n	Particle number density, m^{-3}
P	Pressure, Pa
Q	Turbulence production term due to shear, kg/m s^3
S	Turbulence production term due to interfacial interactions, kg/m s^3
Sc^t	Turbulent Schmidt number, dimensionless, $Sc^t = 0.7$
t	Time, s
T	Temperature, K
$\mathbf{V}$, V , $\mathbf{v}$	Velocity, m/s
We	Weber number, dimensionless

Greek letters

α	Volume fraction, dimensionless
β	Constant in Eq. (15), dimensionless, $\beta = 8.2$
ε	Turbulent kinetic energy dissipation rate, m^2/s^3
μ	Dynamic viscosity, kg/m s
σ	Surface tension, N/m
σ_k	Constant in Eq. (13), dimensionless, $\sigma_k = 1.0$
σ_ε	Constant in Eq. (13), dimensionless, $\sigma_\varepsilon = 1.3$
ρ	Density, kg/m^3
$\boldsymbol{\tau}$	Sheer stress tensor, Pa

Subscripts

br	Break-up
coal	Coalescence
c	Continuous phase
cr	Critical
d	Dispersed phase
drift	Drift velocity
g	Gas
l	Liquid
m	Mixture
vm	Virtual mass

Superscripts

disp	Turbulent dispersion
rel	Relative
t, turb	Turbulent
T	Transpose
'	Fluctuation component

REFERENCES

[1] Pougatch, K., Salcudean, M., Chan, E., and Knapper, B., 2008, "Modelling of Compressible Gas-Liquid Flow in a Convergent-Divergent Nozzle," Chem. Eng. Sci., 63, pp. 4176-4188.

[2] Gray, M. R., 2002, "Fundamentals of Bitumen Coking Processes Analogous to Granulation: a Critical Review," Can. J. Chem. Eng. 80, pp. 393-401.

[3] Pougatch, K., Salcudean, M., Chan, E., and Knapper, B., 2009, "A Two-Fluid Model of Gas-Assisted Atomization Including Flow Through the Nozzle, Phase Inversion, and Spray Dispersion," Int. J. Multiphase Flow, 35, pp. 661-675.

[4] Pougatch, K., and Salcudean, M., 2010, "Numerical Simulation of Liquid Spray Dispersion in a Fluidized Bed," Can. J. Chem. Eng. in press.

[5] Drew, D. A., and Passman, S. L., 1999, Theory of Multicomponent Fluids, Springer, New York.

[6] Kolev, N. I., 2002, Multiphase Flow Dynamics: 1. Fundamentals, Springer, Berlin.

[7] Viollet, P. L. and Simonin, O., 1994, "Modelling Dispersed Two-Phase Flows: Closure Validation and Software Development," App. Mech. Rev., 47 (6, part 2), S80-S84.

[8] Behzadi, A., Issa, R. I., and Rusche, H., 2004, "Modelling of Dispersed Bubble and Droplet Flow at High Phase Fractions," Chem. Eng. Sci., 59, pp. 759-770.

[9] Martinez-Bazan, C., Montanes, J. L., and Lasheras, J. C., 1999, "On the Breakup of an Air Bubble Injected into a Fully Developed Turbulent Flow. Part 1. Breakup frequency," J. Fluid Mech., 401, pp. 157-182.

[10] Kolev, N. I., 2002, Multiphase Flow Dynamics: 2. Thermal and Mechanical Intereactions, Springer, Berlin.

[11] Kocamustafaogullari, G., Smits, S. R., and Razi, J., 1994, "Maximum and mean droplet sizes in annular two-phase flow," Int. J. Heat Mass Transfer, 37, pp. 955-965.

[12] Spalding, D. B., 1980, "Numerical Computation of Multiphase Flow and Heat Transfer," Recent Advances in Numerical Methods in Fluids, Taylor, C., and Morgan, K. eds, Pineridge Press, Swansea, Vol.1, pp.139-168.